NANO LETTERS

pubs.acs.org/NanoLett

Letter

Realization of Curved Circular Nanotubes Using In Situ Monitored Self-Assembly

Zihao Lin, Chunhui Dai, and Jeong-Hyun Cho*

Cite This: *Nano Lett.* 2022, 22, 2140−2146

Read Online

ACCESS | Metrics & More | Article Recommendations | Supporting Information

ABSTRACT: Curved fluidic channels with a circular cross-section play an important role in biology, chemistry, and medicine. However, in nanofluidics, a problem that is largely unsolved is the lack of an effective fabrication method for curved circular nanotubes (10−1000 nm). In this work, an electron-beam-induced self-assembly process was applied to achieve fine curved nanostructures for the realization of nanofluidic devices. The diameter of the tube could be precisely controlled by an atomic layer deposition process. Fluid transported through the nanochannels was verified and characterized using a dark-field microscope under an optical diffraction limit size. The fluid flow demonstrates that the liquid's evaporation (vapor diffusion) in the nanochannel generates compressed vapor, which pumps the liquid and pushes it forward, resulting in a directional flow behavior in the ∼100 nm radius of tubes. This phenomenon could provide a useful platform for the development of diverse nanofluidic devices.

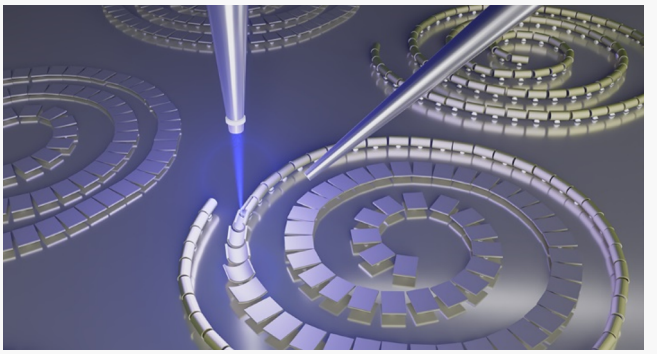

KEYWORDS: *nanofluidic channel, circular tube, self-assembly, in situ*

Diverse shapes of micro- and nanofluidic channels have been studied for various applications, such as biological testing,[1,2] clinical diagnosis,[3,4] environmental analysis,[5] drug synthesis,[6,7] and energy generation.[8,9] In particular, curved (arc on *xy*-plane) microfluidic channels have been extensively investigated since they increase the effective channel length per unit chip length in the flow direction. Simultaneously, a curved microchannel induces a centrifugal force that drives a transverse secondary flow (Dean vortices), which plays a crucial role in cell separation, fluid mixing, and target particle trapping.[10−14] Unlike the micro one, the curved nanochannel exhibits several distinctive properties because of its small feature size, such as higher energy conversion,[15] molecular interaction,[16] and ion transportation.[17] Furthermore, if the channel cross-section is circular instead of the common rectangular one in most micro- and nanofluidic channels, it can eliminate the corner effect that creates nonuniform pressure distributions at the corners of the channel.[18] The nonuniform pressure buildup leads to the accumulation of biological substances near the corner instead of distributing them uniformly.[19,20] The circular cross-section also minimizes the shear stress on biological substances (cells or DNAs) flowing in the channel.[20,21] For these reasons, circular tubes at the nanoscale can be effectively applied in important research fields, such as DNA sampling and analysis,[22] virus detection,[23] and characterization of protein molecules.[24,25] In addition, the theoretical model describing the influence of corner flow on fluid transport is extremely complicated.[26,27] A circular cross-section largely simplifies the complexity of the model and improves the accuracy of theoretical predictions. It is also expected that the circular nanochannels can accurately mimic fluid behavior in root hair and capillaries (many are just under a couple of micrometers) for botany and angiology purposes. Due to these reasons, a strong and effective approach for fabricating a circular nanotube (10−1000 nm) for liquid transportation is in significant demand.

Several ways were reported to achieve circular tubes using gel fiber,[18] silicone oligomers,[19] and templates of molten photoresist.[21,28] However, these methods were only developed for micro- and macroscale channels. Unlike macro- and microscale dimensions, it is extremely difficult to realize circular tubes at the nanoscale because conventional lithographic techniques are based on the projection method,[29] resulting in rectangular cross sections. Moreover, gray-scale lithography does not allow the formation of circular sidewalls on a scale of a few 100s of nm.[30,31] Currently, it has been shown that a novel class of straight circular nanotubes can be formed with a reliable, size adjustable, reproducible, and wafer-scale fabrication method by a strain-induced self-rolling process.[32−34] The mismatch lattice between

Received: October 22, 2021
Revised: January 13, 2022
Published: January 20, 2022

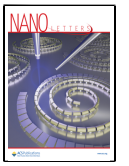

https://doi.org/10.1021/acs.nanolett.1c04093
Nano Lett. 2022, 22, 2140−2146

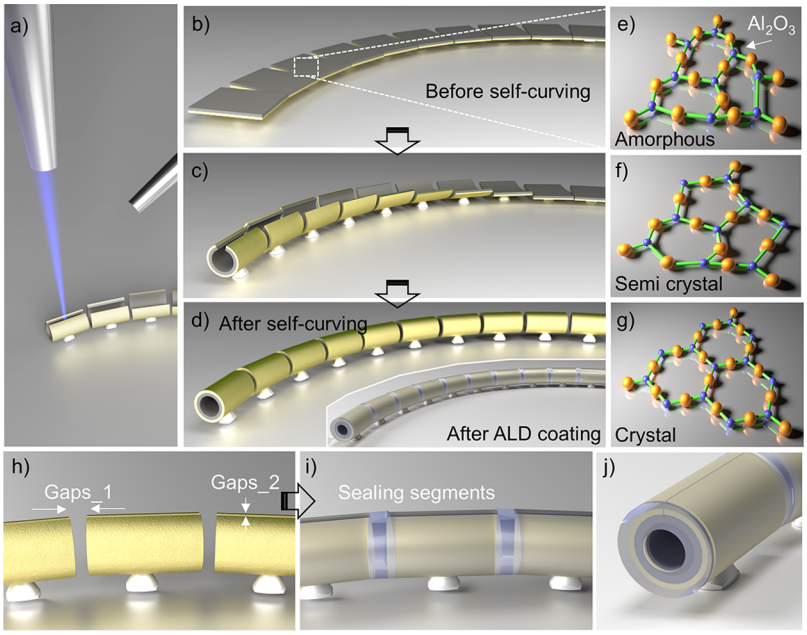

Figure 1. Conceptual sketches of fabricating curved circular nanotubes. (a) Conceptual schematic of the electron-beam-induced self-assembly process. (b) The designed curved 2D patterns before self-curving, (c) during the curving process, and (d) after the self-curving process (inset image shows the 3D curved tubular structure after coating by the ALD process). (e)−(g) Conceptual sketches of Al_2O_3 changing from the amorphous state to the crystalline state under electron beam irradiation. The fabrication process leaves tiny gaps between two adjacent tubes and at the top of each cylinder (h), and (i)−(j) can be sealed after the coating process.

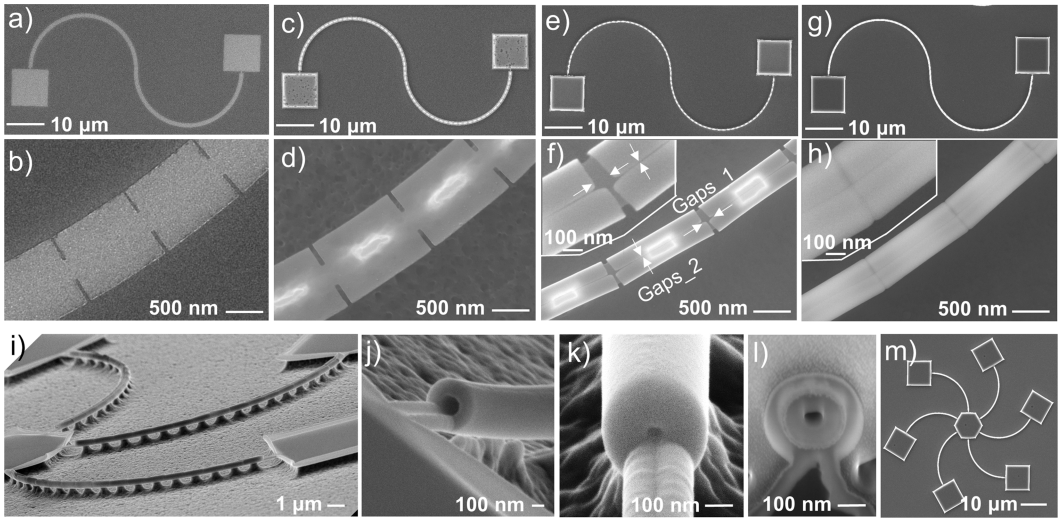

Figure 2. Real fabrication procedures for curved circular nanotubes. Cr and Al_2O_3 were deposited on EBL predefined patterns before (a), (b) and (c), (d) after the RIE process. 3D tubular structure curved by electron-beam-induced curving before (e), (f) and (g), (h) after the ALD sealing process. (i) The sealed tubular structure captured with a large angle. (j) A circular shape cross section of the tube at (j) inlet/outlet after sealing. The diameter of a circular tube is the same at the (k) inlet/outlet and (l) the middle position of a 4 μm tube cut by FIB down to 50 nm. (m) The hexagonal dart shape consists of six curved circular tubes.

two layers induces a stress that achieves self-rolling up from the substrate when the sacrificial layer is selectively wet-etched underneath. This technique offers a flexible way to fabricate nanotubes with diameter ranging from 20 nm to microscale[32] for the applications of fluid transportation[33] and transistor device integration in the wafer scale.[34] More recently, to overcome problems caused by wet etching, such as capillary forces and aggressive reagents, they invented a dry etching method with a new rolling approach. The strained bilayer processes a tensile strain in the top layer and a compressive one at the bottom due to intentionally varying different deposition rates during film growth. By preopening a reactive ion etching (RIE) window, the strained nanomembrane can be released at the final stage and achieve more than 6000 microcapacitors integrated on a wafer scale.[35] However, realizing curved circular nanotubes, which is an important nanofluidic research area, remains a challenge. Here, we introduce a way to realize curved (arc) circular nanotubes with radii of 5−100 nm using an in situ monitored self-curving process (Figure 1), which provides real time images and good controllability of the self-assembly with nanoscale precision. The in situ monitored self-assembly technique also provides a novel way for perfect welding, jointing multiple

https://doi.org/10.1021/acs.nanolett.1c04093
Nano Lett. 2022, 22, 2140−2146

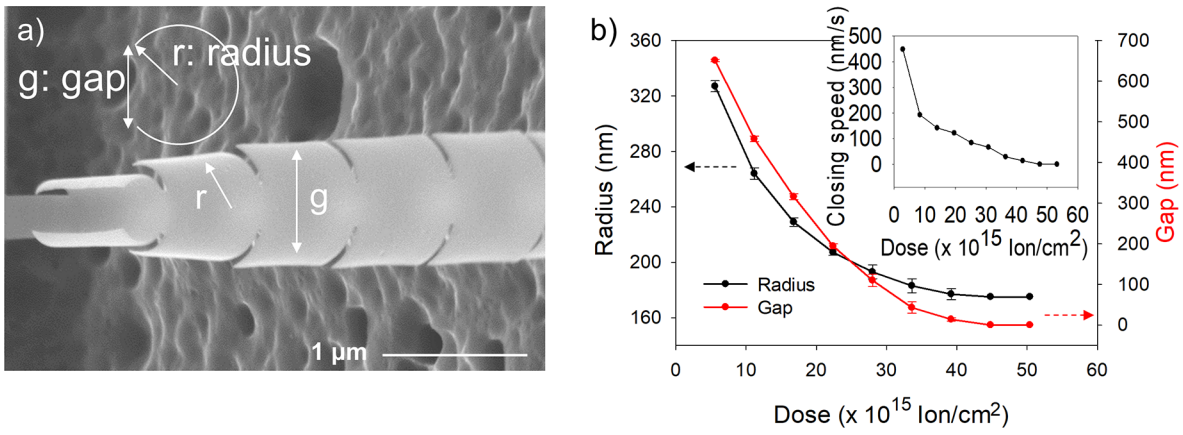

Figure 3. Curving process was in situ monitored and recorded. (a) SEM image was captured during a dynamic self-curving process, which was induced by an electron beam. Here *r* is the radius of the tube, and *g* is the width of the gap. The dose versus radius and width of the gap are in situ monitored in (b), and the closing speed of gap *g* is recorded in the inset.

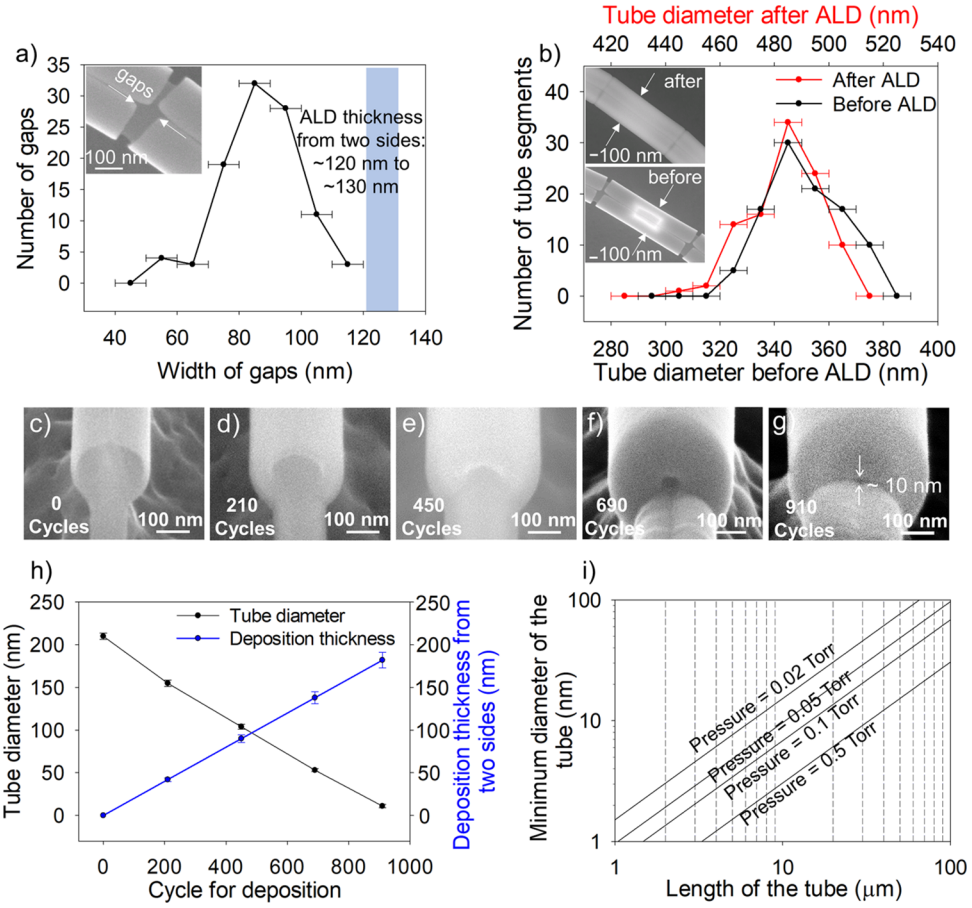

Figure 4. (a) Largest gap width between two tubes after self-assembly vs the number of gaps in each interval; the deposition thickness from two sides is about 120−130 nm. Inset picture shows the measured position. (b) Tube diameter before and after ALD vs the number of tubes in each interval. Inset picture shows the measured position. The ALD sealing process was continuously monitored in (c)−(g) and was plotted in (h). The numerical calculation of atomic layer diffusion length inside a tube of the ALD system was plotted in (i).

nanopieces to form nanocylinders at the nanoscale. The sealing condition and liquid flow in nanocylinders with radii of/under 100 nm were verified using a dark-field microscope system. The proposed technique shown in this paper will provide a useful platform for the development of diverse nanofluidic devices.

In a scanning electron microscope (SEM) system, electrons generated from an electron gun hit and interact with a sample, producing secondary electrons, backscattered electrons, and characteristic X-rays that emit from the sample surface (Figure 1a). These signals are collected by detectors to identify the shape of the sample which is displayed on a SEM monitor. Based on our previous results,[36] Al_2O_3 under proper electron beam irradiation undergoes a phase change from an amorphous state (a-Al_2O_3) to one of the crystalline polymorphic states (α-Al_2O_3) (Figure 1b−g), which causes a volume change of the structure, resulting in a self-assembly (-curving) process. It is worth noting

https://doi.org/10.1021/acs.nanolett.1c04093
Nano Lett. 2022, 22, 2140−2146

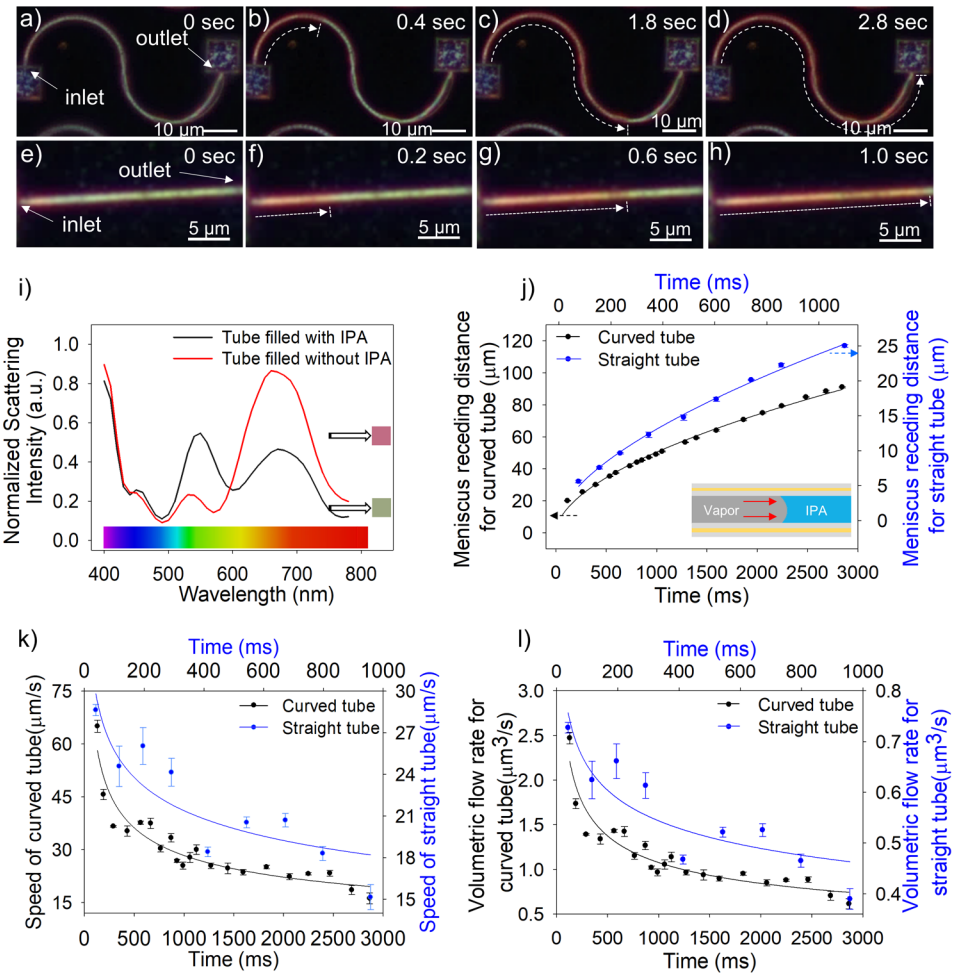

Figure 5. Drying experiment of IPA monitored in (a)−(d) a curved circular tube and (e)−(h) a straight circular tube. Green color indicates the IPA was in the tube, while the orange color indicates that the tube was dried out. The time starts when IPA started to evaporate. (i) Simulated scattering spectra of the tube with and without IPA filling inside. Colors were transformed from each spectrum. Data were normalized to the maximum intensity value in the spectra. (j) The drying time vs meniscus receding distance in straight and curved tubes. Data were fitted in power form. (k) The drying time vs the speed of the flowing liquid measured based on (a)−(h). Data were fitted in power form. (l) The drying time vs volumetric flow rate calculated based on (j) in both the curved and straight tube. Data were fitted in power form.

that other amorphous materials including oxide[37] and metal alloys[38] can also be used for this self-assembly process. To realize curved cylindrical nanostructures using a self-curving process, small rectangular patterns were integrated into a curved 2D structure (Figures 1b and 2a,b). The Si substrate under the patterns was selectively etched using a reactive ion etcher (RIE), leaving anchors of Si to hold up the patterns at the center (Figure 2c,d). Using the in situ monitored self-assembly process, the shape transformation can be carefully controlled. Under e-beam irradiation, the 2D patterns gradually curved up to 3D shape: when the two edges of the nanocylinder are touched, the self-assembly process is automatically stopped due to self-locking, and then circular tubes are completed (segmented curved nanocylinders) (Figures 1b−d and 2e,f). The optimal gap distances between and within each cylinder (Gaps_1 and Gaps_2 in Figures 1h and 2f) were calculated before drawing the design to prevent the edges of the completely curved cylindrical structures from obstructing one another. The gaps (Gaps_1) between cylinders should be as small as possible to realize connections with minimal welding material. This process also leaves tiny gaps (Gaps_2) at the joint part on the top of the tubes (Figures 1h and 2f). Next, a thermal atomic layer deposition (ALD) system was used to completely seal these gaps. Compared with chemical vapor deposition (CVD), which is unable to achieve single atomic layer thickness sealing, suffers from high temperature, contamination, more defects, and inhomogeneous coating:[39−41] this thermal ALD process enables Al_2O_3 to grow from the surface of the tube uniformly with digitized film thickness control, which can easily seal all the gaps but leave enough space for liquid flow inside the tube (Figures 1i,j and 2g,h). This approach finally enables the formation of curved nanocylinders (Figure 2i) with a circular cross section (Figure 2j). It is well possible that the coating thickness may form a gradient from the inlet to the middle part of the tube when the inner diameter becomes much smaller, making a large discrepancy of the inner diameter at different positions along the length of the tube. For certification, by further increasing the cycle of ALD until the diameter of the tube remains only ∼50 nm (Figure 2k), the cross section at the middle of the cylinder (Figure 2l) cut by a focused ion beam (FIB) system shows the same diameter as the one at the end (Figure 2k), which indicates the coating uniformity along the tube. Similarly, a hexagonal dart shape (Figure 2m), consisting of six curved tube structures integrated onto a pad, was also realized, which has potential

https://doi.org/10.1021/acs.nanolett.1c04093
Nano Lett. 2022, 22, 2140−2146

applications for the integration of nanodevices. The step-by-step details of the experimental fabrication process (Figure 2) are described in the Supporting Information (SI, Figure S1). While the sample was irradiated by an electron beam, the curving behavior (radius and gap shown in Figure 3a) was continuously monitored to confirm that all the tube structures were completely curved. Simultaneously, the beam energy (dose) applied for curving was recorded until the 2D patterns were completely curved into cylindrical structures (Figure 3b, see SI for dose calculation). As time moves forward, the dose increases, and the curving speed gradually decreases (Figure 3b, inset). This can be explained by the saturation of Al_2O_3 crystallization, which is the cause of the volume changes and self-curving as discussed.[36] When the dose reaches 50.4×10^{15} ion/cm^2, the radius becomes 175 nm, and the gap is almost 0 nm. At this dose, the edges touch each other, thus the structure stops curving regardless of any further dose increase.

After forming the 3D tubular structures, an Al_2O_3-based ALD process with 600 cycles (in our case 1−1.1 Å per cycle based on different tests results) was performed to completely seal the gaps between tube segments and achieve fluidic transportation inside the structure. The largest gap between every pair of tube segments after the curving process was measured (Figure 4a, measurement position is shown in the inset). The highest number of gaps is between 80 and 90 nm, and the largest gap is less than 120 nm, meaning an ∼65 nm thick Al_2O_3 coating is sufficient to cover all the gaps. The tube diameters before and after ALD were measured to investigate outer diameter changes (Figure 4b). In theory, a 1.1 μm wide 2D pattern corresponds to an approximately 360 nm pipe diameter (5 nm tube thickness is taken into consideration).

Based on the data presented in Figure 4b, the largest number of samples fall in the interval from ∼340 to ∼360 nm before ALD sealing, which is very close to the estimated values (360 nm) obtained from calculations. After the ALD process, the highest peak (∼340 to ∼360 nm) moves to the interval (∼480 to ∼500 nm), which is in accordance with the theoretical diameter (∼480 to ∼490 nm) after 60 cycle. This result indicates that ∼5 nm thick pristine nanocylinders are strong enough to maintain their shape at high temperatures (200 °C) during the ALD process. The inner diameter can be well controlled by the width of 2D patterns and the sealing thickness (ALD coating) before and after self-assembly, respectively. After ALD for 210, 450, 690, and 910 cycles, the diameters were measured based on SEM images (Figure 4c−h). The ALD technique utilizing a self-saturation process is well acknowledged as forming a uniform and stable growth layer with the capability of digitized film thickness control. The self-saturating nature of the surface reactions makes the film thickness controlled at the atomic scale.[42] Thus, the diameter of the tube can be well manipulated from hundreds of nanometers to tens of nanometers accurately depending on the number of ALD cycles (Figure 4h). It is also possible to achieve an inner diameter down to 10 nm (Figure 4g) on a 4 μm long tube segment under 0.5 Torr working pressure with 910 ALD cycles. To estimate the minimum inner diameter achievable with respect to the length of each tube segment, a numerical analysis was carried out (Figure 4i, see SI for the detailed numerical calculation). Based on the results shown in Figure 4i, the minimum inner diameter depends on the aspect ratio as well as pressure. Under the same working pressure, it can be shown that an inner diameter of 10 nm can be realized with a short tube length (Figure 4g). From the cross-sectional SEM images, it is also verified that inner diameters along the entire tubes are uniform (Figure 2k,l, due to the resolution limit of SEM and 10−20 nm deformation resulting from FIB cutting an ion bombardment process;[43,44] tubes with ∼25 nm radius were selected instead of 10 nm for verification). To confirm that the gaps are fully sealed without leakage and the tubes can work as liquid nanochannels, fluid transportation was demonstrated and characterized using a dark-field microscope under the optical diffraction limit size (Figure 5). Under the dark-field microscope, nanochannels acting as "bulbs" can be lit up when liquid (isopropyl alcohol, IPA, acting as "current") flows in an approximately 110 nm radius of curved tube (Figure 5a−d) and an approximately 90 nm radius of straight tube (Figure 5e−h) (see detailed experimental operating procedures under the dark field in the SI). Consider 0 s as the beginning of liquid flowing from the inlet: after 2.8 s, the IPA flows (dries out) from one side to the other side in the curved circular tube (Figure 5a−d). Similarly, images show IPA flowing from the left to the right side in the straight tube in 1.0 s (Figure 5e−h). This proves the transport capability inside the circular nanotube structures. In addition, the boundary between the air and liquid moving from the inlet to the outlet proves that there is no leakage in the middle of the nanotubes when passing across gaps (Figure 2f). The color of the tube changing from green (when there is liquid in the tube) to orange (when there is air in the tube) is due to different refractive indices inside the tube, corresponding to different optical responses. The color change was further verified by a 3D finite-difference time-domain simulator (Lumerical FDTD Solutions[45] see SI (Figure S2) for detailed configuration) and a color calculator software (Figure 5i). The simulation result indicates that a strong scattering peak at 550 nm and a weak one appear at approximately 680 nm when IPA is inside the tube; this spectrum represents a green color. A tube with air shows a major peak at 680 nm representing a red color. The colors obtained from the simulation results (Figure 5i) are almost the same as the ones we obtained via dark-field experiment (Figure 5a−h), this strongly confirms the hypothesis of fluid transport inside the tube. For the characterization of the fluid flowing in the straight and curved nanotubes, the flow traces (Figure 5a−h) of the liquid were obtained from the video frames and then converted to meniscus receding distance (Figure 5j), speed (Figure 5k), and volumetric flow rate (Figure 5l) at each time section (a real-time monitored video is also provided in SI Video 1). As the time increases, the receding distance of the meniscus does not have a constant change in time for either the straight or curved tube (Figure 5j); this is in accordance with the results shown in Figure 5k−l: the flow speed and volumetric flow rate decrease sharply at the beginning and then flatten until the end. We attribute part of this fluidic behavior to the vapor diffusion process,[46] which shows a similar receding tendency of the meniscus as observed by our experiment. However, a pure vapor diffusion process should occur from both ends, whereas ours only diffuses from one side (Figure 5a−h). Thus, this directional meniscus receding behavior cannot be explained by diffusion only. A conjecture is proposed here: IPA is a very volatile liquid. When IPA is confined inside the nanotube and starts to evaporate, its vapor which is imprisoned under such a small volume is likely being "compressed". The compressed vapor pumps the liquid and pushes it forward, which leads to this directional migration behavior in the ∼100 nm radius of tubes. It is worth noting that, to the best of our knowledge, this new phenomenon was not reported previously; however, this new phenomenon could provide a useful platform for the development of diverse nanofluid devices. A manuscript for the detailed

https://doi.org/10.1021/acs.nanolett.1c04093
Nano Lett. 2022, 22, 2140−2146

mechanism of the liquid flow in the circular nanotubes with sub-100 nm dimension is under preparation in our lab.

In conclusion, a fabrication approach for a curved circular nanotube with a radius at 100 nm scale has been developed via an electron-beam-induced self-assembly process. SEM enables nanoscale precise control for curving 2D patterns into 3D curved nanocylinders with perfect circular cross section. The inner diameter of the nanocylinders can be adjusted down to 10 nm with a precision of 0.1 nm using an ALD process. Although the developed e-beam-based self-curving technique still remains challenging due to its low efficiency and unparallel manufacturing for the wafer scale, which needs to be overcome in the future, the fabrication technique shown in this paper will shed light on an approach for fabricating both curved and straight circular tubes under a 100 nm scale with fast adjustable tubular size and radii of curvature and provide an effective platform for researching nanofluidics via dark-field color rendering. Moreover, the novel fluid flow generated by a self-pumping process might trigger diverse applications that require mechanical power or force in nanoscale devices.

■ ASSOCIATED CONTENT

Supporting Information

The Supporting Information is available free of charge at: . Video 1: (MP4) Video 2: (MP4) The Supporting Information is available free of charge at https://pubs.acs.org/doi/10.1021/acs.nanolett.1c04093.

The real-time video of an IPA evaporation process inside the curved tube under a dark-field microscope (MP4)

The real-time video of an IPA evaporation process inside the straight tube under a dark-field microscope (MP4)

Fabrication of sealed curved circular nanofluidic channel, experiment on focused-ion-beam-based cutting process, SEM dose calculation, theory model of the diffusion length inside the tube, dark-field microscope-based experiment, simulation model design description, and numerical simulation of the light-scattering effect based on the sample under a dark-field microscope (PDF)

■ AUTHOR INFORMATION

Corresponding Author

Jeong-Hyun Cho − *Department of Electrical and Computer Engineering, University of Minnesota, Minneapolis, Minnesota 55455, United States;* orcid.org/0000-0003-2870-1960; Email: jcho@umn.edu

Authors

Zihao Lin − *Department of Electrical and Computer Engineering, University of Minnesota, Minneapolis, Minnesota 55455, United States*

Chunhui Dai − *Department of Electrical and Computer Engineering, University of Minnesota, Minneapolis, Minnesota 55455, United States*

Complete contact information is available at: https://pubs.acs.org/10.1021/acs.nanolett.1c04093

Notes

The authors declare no competing financial interest.

■ ACKNOWLEDGMENTS

This research was supported by the National Science Foundation under Grant No. CMMI-1454293. Portions of this work were conducted in the Minnesota Nano Center, which is supported by the National Science Foundation through the National Nanotechnology Coordinated Infrastructure (NNCI) under Award Number ECCS-2025124. Part of this work was carried out in the College of Science and Engineering Characterization Facility, University of Minnesota, which has received capital equipment funding from the National Science Foundation through the UMN MRSEC under Award Number DMR-2011401.

■ REFERENCES

(1) Xia, Y.; Si, J.; Li, Z. Fabrication Techniques for Microfluidic Paper-Based Analytical Devices and Their Applications for Biological Testing: A Review. *Biosens. Bioelectron.* **2016**, *77*, 774−789.

(2) Vázquez-Guardado, A.; Mehta, F.; Jimenez, B.; Biswas, A.; Ray, K.; Baksh, A.; Lee, S.; Saraf, N.; Seal, S.; Chanda, D. DNA-Modified Plasmonic Sensor for the Direct Detection of Virus Biomarkers from the Blood. *Nano Lett.* **2021**, *21*, 7505−7511.

(3) Ma, Y.-H. V.; Middleton, K.; You, L.; Sun, Y. A Review of Microfluidic Approaches for Investigating Cancer Extravasation During Metastasis. *Microsyst. Nanoeng.* **2018**, *4*, 1−13.

(4) Huang, Y. L.; Segall, J. E.; Wu, M. Microfluidic Modeling of the Biophysical Microenvironment in Tumor Cell Invasion. *Lab Chip* **2017**, *17*, 3221−3233.

(5) Kudr, J.; Zitka, O.; Klimanek, M.; Vrba, R.; Adam, V. Microfluidic Electrochemical Devices for Pollution Analysis−a Review. *Sens. Actuators, B* **2017**, *246*, 578−590.

(6) Lu, M.; Ozcelik, A.; Grigsby, C. L.; Zhao, Y.; Guo, F.; Leong, K. W.; Huang, T. J. Microfluidic Hydrodynamic Focusing for Synthesis of Nanomaterials. *Nano Today* **2016**, *11*, 778−792.

(7) Ahn, J.; Ko, J.; Lee, S.; Yu, J.; Kim, Y.; Jeon, N. L. Microfluidics in Nanoparticle Drug Delivery; from Synthesis to Pre-Clinical Screening. *Adv. Drug Delivery Rev.* **2018**, *128*, 29−53.

(8) Shi, Q.; Wang, H.; Wang, T.; Lee, C. Self-Powered Liquid Triboelectric Microfluidic Sensor for Pressure Sensing and Finger Motion Monitoring Applications. *Nano Energy* **2016**, *30*, 450−459.

(9) Nie, J.; Ren, Z.; Shao, J.; Deng, C.; Xu, L.; Chen, X.; Li, M.; Wang, Z. L. Self-Powered Microfluidic Transport System Based on Triboelectric Nanogenerator and Electrowetting Technique. *ACS Nano* **2018**, *12*, 1491−1499.

(10) Zhao, Q.; Yuan, D.; Zhang, J.; Li, W. A Review of Secondary Flow in Inertial Microfluidics. *Micromachines* **2020**, *11*, 461.

(11) Yuan, D.; Zhao, Q.; Yan, S.; Tang, S.-Y.; Alici, G.; Zhang, J.; Li, W. Recent Progress of Particle Migration in Viscoelastic Fluids. *Lab Chip* **2018**, *18*, 551−567.

(12) Squires, T. M.; Quake, S. R. Microfluidics: Fluid Physics at the Nanoliter Scale. *Rev. Mod. Phys.* **2005**, *77*, 977.

(13) Razavi Bazaz, S.; Rouhi, O.; Raoufi, M. A.; Ejeian, F.; Asadnia, M.; Jin, D.; Ebrahimi Warkiani, M. 3D Printing of Inertial Microfluidic Devices. *Sci. Rep.* **2020**, *10*, 1−14.

(14) Liu, C.; Zhang, W.; Li, Y.; Chang, J.; Tian, F.; Zhao, F.; Ma, Y.; Sun, J. Microfluidic Sonication to Assemble Exosome Membrane-Coated Nanoparticles for Immune Evasion-Mediated Targeting. *Nano Lett.* **2019**, *19*, 7836−7844.

(15) Liu, Y.; Jian, Y.; Yang, C. Electrochemomechanical Energy Conversion Efficiency in Curved Rectangular Nanochannels. *Energy* **2020**, *198*, 117401.

(16) Wang, M.; Meng, H.; Wang, D.; Yin, Y.; Stroeve, P.; Zhang, Y.; Sheng, Z.; Chen, B.; Zhan, K.; Hou, X. Dynamic Curvature Nanochannel-Based Membrane with Anomalous Ionic Transport Behaviors and Reversible Rectification Switch. *Adv. Mater.* **2019**, *31*, 1805130.

(17) Duan, C.; Majumdar, A. Anomalous Ion Transport in 2-nm Hydrophilic Nanochannels. *Nat. Nanotechnol.* **2010**, *5*, 848−852.

(18) Ng, P. F.; Lee, K. I.; Yang, M.; Fei, B. Fabrication of 3D PDMS Microchannels of Adjustable Cross-Sections via Versatile Gel Templates. *Polymers* **2019**, *11*, 64.

(19) Fiddes, L. K.; Raz, N.; Srigunapalan, S.; Tumarkan, E.; Simmons, C. A.; Wheeler, A. R.; Kumacheva, E. A Circular Cross-Section PDMS Microfluidics System for Replication of Cardiovascular Flow Conditions. *Biomaterials* **2010**, *31*, 3459−3464.
(20) Yang, X.; Forouzan, O.; Burns, J. M.; Shevkoplyas, S. S. Traffic of Leukocytes in Microfluidic Channels with Rectangular and Rounded Cross-Sections. *Lab Chip* **2011**, *11*, 3231−3240.
(21) Huang, Z.; Li, X.; Martins-Green, M.; Liu, Y. Microfabrication of Cylindrical Microfluidic Channel Networks for Microvascular Research. *Biomed. Microdevices* **2012**, *14*, 873−883.
(22) Lam, E. T; Hastie, A.; Lin, C.; Ehrlich, D.; Das, S. K; Austin, M. D; Deshpande, P.; Cao, H.; Nagarajan, N.; Xiao, M.; Kwok, P.-Y. Genome Mapping on Nanochannel Arrays for Structural Variation Analysis and Sequence Assembly. *Nat. Biotechnol.* **2012**, *30*, 771−776.
(23) Berkenbrock, J. A.; Grecco-Machado, R.; Achenbach, S. Microfluidic Devices for the Detection of Viruses: Aspects of Emergency Fabrication During the Covid-19 Pandemic and Other Outbreaks. *Proc. Royal Soc. A* **2020**, *476*, 20200398.
(24) Wang, Y.-C.; Stevens, A. L.; Han, J. Million-Fold Preconcentration of Proteins and Peptides by Nanofluidic Filter. *Anal. Chem.* **2005**, *77*, 4293−4299.
(25) Dai, C.; Lin, Z.; Agarwal, K.; Mikhael, C.; Aich, A.; Gupta, K.; Cho, J.-H. Self-Assembled 3D Nanosplit Rings for Plasmon-Enhanced Optofluidic Sensing. *Nano Lett.* **2020**, *20*, 6697−6705.
(26) Eijkel, J. C.; Dan, B.; Reemeijer, H.; Hermes, D.; Bomer, J. G.; van den Berg, A. Strongly Accelerated and Humidity-Independent Drying of Nanochannels Induced by Sharp Corners. *Phys. Rev. Lett.* **2005**, *95*, 256107.
(27) Laine-Pearson, F.; Hydon, P. Particle Transport in a Moving Corner. *J. Fluid Mech.* **2006**, *559*, 379−390.
(28) Wang, G.-J.; Ho, K.-H.; Hsu, S.-h.; Wang, K.-P. Microvessel Scaffold with Circular Microchannels by Photoresist Melting. *Biomed. Microdevices* **2007**, *9*, 657−663.
(29) Chen, Y.; Shu, Z.; Zhang, S.; Zeng, P.; Liang, H.; Zheng, M.; Duan, H. Sub-10-nm Fabrication: Methods and Applications. *Int. J. Extrem. Manuf.* **2021**, *3*, 032002.
(30) Nakano, T.; Itoyama, T.; Yoshida, K.; Sawada, Y.; Ikeda, S.; Fukuda, T.; Matsuda, T.; Negoro, M.; Arai, F. Multiscale Fabrication of a Transparent Circulation Type Blood Vessel Simulator. *Biomicrofluidics* **2010**, *4*, 046505.
(31) He, R.; Yunus, D.; Uhl, C.; Shi, W.; Sohrabi, S.; Liu, Y. Fabrication of Circular Microfluidic Channels through Grayscale Dual-Projection Lithography. *Microfluid. Nanofluid.* **2017**, *21*, 13.
(32) Deneke, C.; Schmidt, O. G. Lithographic Positioning, Areal Density Increase and Fluid Transport in Rolled-up Nanotubes. *Phys. E* **2004**, *23*, 269−273.
(33) Deneke, C.; Schmidt, O. G. Real-Time Formation, Accurate Positioning, and Fluid Filling of Single Rolled-up Nanotubes. *Appl. Phys. Lett.* **2004**, *85*, 2914−2916.
(34) Grimm, D.; Bof Bufon, C. C.; Deneke, C.; Atkinson, P.; Thurmer, D. J.; Schäffel, F.; Gorantla, S.; Bachmatiuk, A.; Schmidt, O. G. Rolled-up Nanomembranes as Compact 3D Architectures for Field Effect Transistors and Fluidic Sensing Applications. *Nano Lett.* **2013**, *13*, 213−218.
(35) Saggau, C. N.; Gabler, F.; Karnaushenko, D. D.; Karnaushenko, D.; Ma, L.; Schmidt, O. G. Wafer-Scale High-Quality Microtubular Devices Fabricated via Dry-Etching for Optical and Microelectronic Applications. *Adv. Mater.* **2020**, *32*, 2003252.
(36) Dai, C.; Li, L.; Wratkowski, D.; Cho, J.-H. Electron Irradiation Driven Nanohands for Sequential Origami. *Nano Lett.* **2020**, *20*, 4975−4984.
(37) Stefanovich, G.; Pergament, A.; Velichko, A.; Stefanovich, L. Anodic Oxidation of Vanadium and Properties of Vanadium Oxide Films. *J. Phys.: Condens. Matter* **2004**, *16*, 4013.
(38) Nagase, T.; Umakoshi, Y. Electron Irradiation Induced Crystallization of the Amorphous Phase in Zr65. 0al7. 5ni10. 0cu17. 5 Metallic Glass. *Sci. Technol. Adv. Mater.* **2004**, *5*, 57.
(39) Swihart, M.; Nijhawan, S.; Mahajan, M.; Suh, S.; Girshick, S. Modeling the Nucleation Kinetics and Aerosol Dynamics of Particle Formation during CVD of Silicon from Silane. *J. Aerosol Sci.* **1998**, *29*, 79−80.
(40) Chang Liu; Yu-Chong Tai. Sealing of Micromachined Cavities Using Chemical Vapor Deposition Methods: Characterization and Optimization. *J. Microelectromech. Syst.* **1999**, *8*, 135−145.
(41) Kühnhold, S.; Saint-Cast, P.; Kafle, B.; Hofmann, M.; Colonna, F.; Zacharias, M. High-Temperature Degradation in Plasma-Enhanced Chemical Vapor Deposition Al_2O_3 Surface Passivation Layers on Crystalline Silicon. *J. Appl. Phys.* **2014**, *116*, 054507.
(42) Cremers, V.; Puurunen, R. L.; Dendooven, J. Conformality in Atomic Layer Deposition: Current Status Overview of Analysis and Modelling. *Appl. Phys. Rev.* **2019**, *6*, 021302.
(43) Ding, X.; Lim, G.; Cheng, C.; Butler, D. L.; Shaw, K.; Liu, K.; Fong, W. Fabrication of a Micro-Size Diamond Tool Using a Focused Ion Beam. *J. Micromech. Microeng.* **2008**, *18*, 075017.
(44) Placet, V.; Méteau, J.; Froehly, L.; Salut, R.; Boubakar, M. L. Investigation of the Internal Structure of Hemp Fibres Using Optical Coherence Tomography and Focused Ion Beam Transverse Cutting. *J. Mater. Sci.* **2014**, *49*, 8317−8327.
(45) *ANSYS/LUMERICAL Home Page*. https://www.lumerical.com/products/fdtd/ (accessed 2021−12−23).
(46) Xie, Q.; Xiao, S.; Duan, C. Geometry-Dependent Drying in Dead-End Nanochannels. *Langmuir* **2017**, *33*, 8395−8403.

https://doi.org/10.1021/acs.nanolett.1c04093
Nano Lett. 2022, 22, 2140−2146